

Journal of Materials Chemistry A

Accepted Manuscript



This is an *Accepted Manuscript*, which has been through the Royal Society of Chemistry peer review process and has been accepted for publication.

Accepted Manuscripts are published online shortly after acceptance, before technical editing, formatting and proof reading. Using this free service, authors can make their results available to the community, in citable form, before we publish the edited article. We will replace this *Accepted Manuscript* with the edited and formatted *Advance Article* as soon as it is available.

You can find more information about *Accepted Manuscripts* in the [Information for Authors](#).

Please note that technical editing may introduce minor changes to the text and/or graphics, which may alter content. The journal's standard [Terms & Conditions](#) and the [Ethical guidelines](#) still apply. In no event shall the Royal Society of Chemistry be held responsible for any errors or omissions in this *Accepted Manuscript* or any consequences arising from the use of any information it contains.

Importance of Open, Heteroatom-Decorated Edges in Chemically-Doped-Graphene for Supercapacitor Applications

Cite this: DOI: 10.1039/x0xx00000x

Received 00th January 2012,
Accepted 00th January 2012

DOI: 10.1039/x0xx00000x

www.rsc.org/

Kazunori Fujisawa,^a Rodolfo Cruz-Silva,^b Kap-Seung Yang,^c Yoong Ahm Kim,^{c,*} Takuya Hayashi,^a Morinobu Endo,^b Mauricio Terrones,^{b,d} Mildred S. Dresselhaus^e

Chemically doped graphene has been actively investigated as electrode material for achieving high-performance electrochemical systems. However, the stability of pure-carbon-rich edges and/or heteroatom-decorated edges, and their effect on the electrochemical performance remains largely unexplored. We found that in a high temperature thermal doping process, the functionalized graphene edges were structurally stable at 1200°C, whereas the edges at 1500°C were unstable and coalesced into loops through covalent bond formation between adjacent graphenes. Interestingly, boron and nitrogen co-doped graphene prepared at 1200°C showed the largest capacitance in both an acidic and an alkaline media due to the presence of the BNO moieties along the edge sites. The doped material also showed the best rate capability due to the largely enhanced electrical conductivity originating from the substitutionally-doped boron and nitrogen atoms. Our findings regarding the stability of heteroatom-decorated edges without looping formation can now be utilized as a guideline for maximizing the electrochemical activity of graphene in various electrochemical systems.

Introduction

In recent years, the two-dimensional sp^2 -hybridized carbon, called “graphene” has been considered one of the most attractive materials for various applications because of its outstanding and unique physical and chemical properties (*e.g.*, superior electric and thermal conductivity, good chemical stability, and mechanical strength).^{1,2} Moreover, a high specific surface area (up to 2630 m²/g) arising from its atomic thickness allows graphene to be an ideal electrode material for electrochemical systems.³⁻⁶ Supercapacitors store energy via the simple adsorption and desorption of electrolyte ions on a high surface area electrode. Up to now, activated carbons with large surface areas of 1000-2000 m²/g have been used as electrode materials for commercial supercapacitors.^{7,8} In the case of activated carbon-based supercapacitors, solvated ions do not undergo a fast charge/discharge process, because of a limited ion diffusion rate caused by relatively small pores as well as a low electrical conductivity coming from their small crystalline size.⁹ In contrast, graphene shows a low diffusion resistance (all carbon atoms are exposed to the surface) and a high electrical conductivity due to its large lateral size. Graphene is more chemically stable than activated carbons and consequently, supercapacitors made with graphene-based materials are expected to have a longer lifetime. Thus, graphene-based materials have been intensively examined as electrode materials for supercapacitor applications where a high current density is strongly desired (*e.g.*, for electric vehicles).¹⁰⁻¹⁵

The most characteristic feature of graphene is the presence of chemically active edge sites. It has been theoretically and experimentally confirmed that graphene chemically active edges with dangling bonds show a different electronic structure as compared with that of the basal-plane.¹⁶⁻¹⁸ Zigzag-edges with a flat band near the Fermi level are known to have a much higher chemical reactivity than armchair-edges. Edges in graphite and graphene systems have shown a 4-10 times larger capacitance than the basal-plane itself.¹⁹⁻²³ These highly chemical reactive edges are likely to be stabilized by reacting with heteroatoms. In addition, as an alternative tool for improving the electrochemical performance of various carbon materials (*e.g.*, activated carbons, carbon nanotubes, and graphenes), heteroatom doping has been carried out by introducing nitrogen,²⁴⁻³⁰ sulfur,³¹ phosphorus,³² boron,^{26-30,33-35} and oxygen.^{36,37} In an ideal case, the edges in graphene could be fully exposed to the surface (fully accessible to an electrolyte) without bending or looping; they could also be decorated with heteroatoms. However, the stability of pure-carbon-edges and/or heteroatom-decorated edges on the electrochemical behaviour for supercapacitor applications are still unexplored, and we aim here at clarifying these issues.

In this study boron- (B-), nitrogen- (N-) and also nitrogen-boron (NB-) co-doped graphene samples were prepared by subjecting graphene oxide to nitrogen plasma, followed by a subsequent thermal treatment in a boron rich environment at 1200 and 1500°C. These prepared chemically doped graphene samples were characterized as well as their electrochemical performance. Several reasons for selecting high-temperature-thermal-diffusion as a simultaneous way of doping and

graphene-oxide reduction are: (1) being able to prepare repeatedly undoped and doped graphene samples from the same precursor (graphene oxide) exhibiting the same specific surface area and degree of crystallinity; (2) to provide stable edge sites, because edge sites are thermally unstable and are eventually converted to stable single- and/or multi-loops around 1500°C; (3) to generate specific B- and/or N-regions that are stable at high temperature, and (4) to provide high electrical conductivity by the introduction of B- and N-atoms into the graphene lattice.

Results and discussion

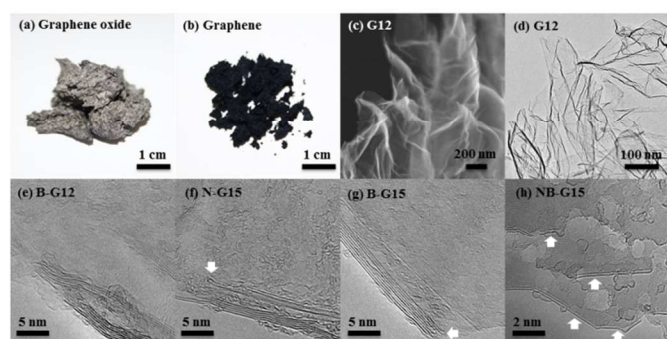


Fig. 1 Photographs of graphene oxide (a) and thermally reduced graphene (b). FE-SEM (c) and TEM (d) images of thermally reduced graphene at 1200°C. (e) High resolution TEM image of boron-doped graphene at 1200°C. High resolution TEM images of nitrogen-(f), boron-(g) and nitrogen-boron (h) doped graphenes at 1500°C. Note that short white arrows in Figs. 1 (f, g and h) indicate the formation of single loops.

Graphene oxide (GO) samples prepared via a modified Hummers method³⁸ were thermally reduced and/or doped using a high temperature thermal process. Since three-dimensional stacking occurs for reduced GO above 2000°C³⁹, and a substantial amount of N atoms are released from carbon materials above 1500°C,⁴⁰ thermal reduction was carried out at 1200 and 1500°C using a graphite furnace. Samples labelled as G12 and G15 represent the thermally reduced graphenes at 1200 and 1500°C, respectively. In order to dope graphene with nitrogen atoms, GO was irradiated with a nitrogen RF-plasma (100 W) for 30 min and were then thermally treated at 1200 and 1500°C using a graphite furnace. N-G12 and N-G15 corresponds those samples that were prepared by nitrogen plasma followed by high temperature thermal reduction at 1200 and 1500°C, respectively. For boron doping, the reagent mixture (GO and boric acid (5 wt. %)) was thermally treated using a graphite furnace. B-G12 and B-G15 indicate samples that were prepared by thermally treating GO and the boric acid mixture at 1200 and 1500°C, respectively. Nitrogen and boron-co-doped graphene was also prepared by combining the nitrogen plasma treatment and the high-temperature boron doping. NB-G12 and NB-G15 correspond to samples that were prepared by thermally heating the nitrogen-plasma treated GO and boric acid mixture at 1200 and 1500°C, respectively. The grey colored GO shows a sponge-like structure (Fig. 1(a)). During thermal reduction and doping, the GO lost almost 70% of its weight, and the resulting material was then converted into graphene by releasing CO or CO₂ from the oxygen functionalities of the GO. The thermally reduced (or undoped) and the doped graphene samples were black-coloured powders (Fig. 1 (b)). In order to observe textural changes caused by doping, FE-SEM and HR-TEM observations on the undoped and doped graphenes were carried out. All graphene samples

show a flat and sheet-like morphology (Fig. 1 (c)), and have a rippled and disordered structure (Fig. 1 (d)). In addition, they have 5-9 multilayers (Fig. 1 (e)). Single-layered reduced GO sheets are likely to stack and then form few layered graphene via strong π - π interaction during the thermal reduction and/or doping processes. Generally, it is not easy to find any distinctive change in the texture between undoped and heteroatom-doped graphenes (see Figs. S1-S3). However, we found a subtle temperature-dependent difference when studying the edge morphologies. Specifically, edges in graphene samples that are prepared at 1200°C are open (not closed) (Fig. 1 (e)), but, edges in graphene materials prepared at 1500°C are structurally converted to “single loops” by covalently bonding adjacent graphene layers (Fig. 1 (f) and (g)). In addition, we observed the predominant formation of “single loops” via the loss of active edges as witnessed by TEM (see Fig. 1 (h)).

Table 1 Elemental compositions and porosity parameters of undoped and doped graphenes.

Sample I.D.	HTT (°C)	Dopant	Composition (at. %)				S_{BET} (m ² /g)	V_{total} (cm ³ /g)	V_{micro} (cm ³ /g) ^a	V_{ext} (cm ³ /g) ^b
			O	C	B	N				
G12	-	-	1.54	98.47	-	-	343	1.60	0.14	1.16
B-G12	1200	B	3.67	93.77	2.56	-	301	1.50	0.12	1.37
N-G12		N	1.80	97.67	-	0.54	342	1.59	0.14	1.45
NB-G12		N-B	2.85	93.74	2.39	1.02	341	1.34	0.14	1.20
G15	-	-	2.94	97.06	-	-	195	0.66	0.08	0.58
B-G15	1500	B	2.71	95.55	1.74	-	121	0.39	0.05	0.35
N-G15		N	2.08	97.56	-	0.36	222	0.81	0.09	0.72
NB-G15		N-B	1.00	96.23	1.98	0.79	168	0.60	0.06	0.54

^a V_{micro} is determined by the Horvath-Kawazoe method. ^b $V_{\text{ext}} = V_{\text{total}} - V_{\text{micro}}$

In order to evaluate the amount and types of chemical functionalities in doped graphene samples, X-ray photoelectron spectroscopy (XPS) measurements were carried out. The elemental composition of the undoped and doped graphene materials is summarized in Table 1. According to the doping method and temperature, the amount of boron atoms varies from 1.74 to 2.56 atomic %, whereas the amount of nitrogen atoms ranges from 0.54 to 1.02 atomic %. However, the amount of nitrogen in NB co-doped graphene samples (i.e., NB-G12 and NB-G15) is two times larger than that of N-doped graphene materials. Such difference can be explained by the B-N bonding in NB codoped graphene sample. To monitor the change in the type of functionalities in more detail, we scrutinized the narrow-scan C 1s, B 1s and N 1s spectra of undoped and doped graphenes that were prepared at 1200 and 1500°C, respectively. The strongest C 1s peak has a maximum around 284.4 eV and can be assigned to sp^2 -hybridized carbon atoms (Fig. 2 (a)). A clear downshift in the binding energy of the C=C assigned peak in B-G12 and a subtle upshift in the binding energy of the C=C assigned peak in N-G12, can be explained by the substitutional introduction of boron and nitrogen atoms at the trigonal sites of graphenes, respectively.^{41, 42} The lack of a change in the binding energy of the C=C peak in NB-G12 can be explained by the offsetting effect of the substitutionally introduced boron and nitrogen atoms. Moreover, when looking at the tail of the C 1s spectra in detail (Fig. 2 (a)), we found no significant change in the peak shape or intensity between undoped and doped graphenes. Such results indicate that all samples have a similar content of oxygen functionalities (C-O bonding).

The B 1s spectra of B-G12 and NB-G12 were deconvoluted into 6 and 7 peaks, respectively. The peaks at 186.0, 187.0 and 188.0 eV correspond to boron carbide (B₄C), boron-cluster (metallic boron) and substituted boron (boron in the graphene lattice, BC₃), respectively.⁴³ For boron doping, boric acid was the chosen dopant, and thus the other peaks correspond to partially or fully oxidized boron. The peaks at 189.9 eV, 190.8

eV and 193.6 eV can be assigned to BC_2O , BCO_2 , and B_2O_3 , respectively.⁴⁴ Since these BCO moieties (BC_2O , BCO_2) are unstable within the graphene lattice, these moieties must be preferentially located at the chemically active edges.

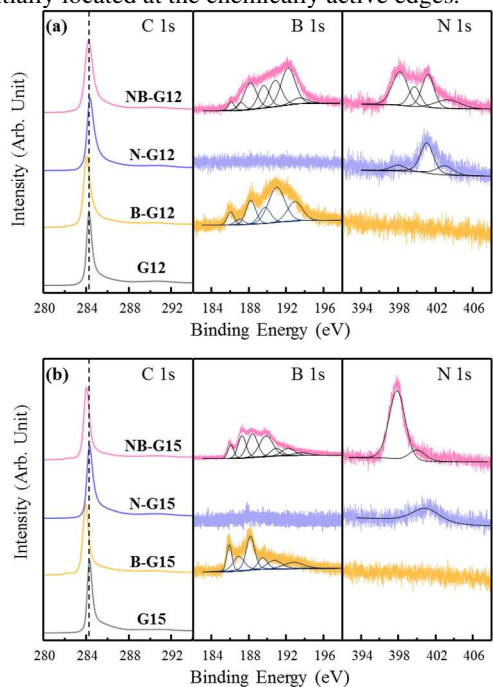


Fig.2 Narrow-scan C 1s, B 1s and N 1s X-ray photoelectron spectroscopy of undoped and doped graphenes that are prepared at 1200°C (a) and 1500°C (b). The dashed line at 284.2 eV indicates the position of graphitic carbon (sp^2).

The peak at 189.9 eV in NB-G12 is more intense than that of B-G12, indicating that this peak is coming from BN bonding as well as BC_2O bonding, as observed by the previously reported position of the BN bonding for boron nitride.⁴⁵ However, the assignment of the strong peak at 192.0 eV for NB-G12 is ambiguous. The absence of such a peak in B-G12 indicates that this peak could be related to nitrogen and boron bonding. In addition, the binding energy is far from that for metallic boron, but close to the one for its oxidized compounds, such as B_2O_3 . Thus this peak could also be related to oxygen. In XPS analysis,

when boron is bonded to oxygen, the upshift in the binding energy of boron occurs due to the high electronegative nature of oxygen. For these reasons, it is expected that this peak appearing at around 192.0 eV corresponds to the BNO moieties, such as BN_2O and BNO_2 , which could be energetically stabilized at the edges such as the BCO moiety.^{45, 46}

The N 1s spectra in N-G12 and NB-G12 shown in Fig. 2 (a) were deconvoluted into 3 and 4 peaks, respectively. The peaks at 398.2 eV, 401.2 eV and 403.2 eV can be assigned to pyridinic nitrogen (N_P), quaternary nitrogen (N_Q : nitrogen in the graphene lattice or at a valley site of the graphene edge), and oxidized nitrogen (N_OX), respectively.^{47, 48} An intense peak located at 398.2 eV in NB-G12 can be explained by BN bonding as well as pyridinic nitrogen. This peak position is in agreement with the previously reported binding energy of nitrogen in boron nitride.⁴⁵ A new peak around 399.8 eV is only observed in NB-G12. In the nitrogen-doped carbon system, this peak can be assigned to pyrrolic nitrogen, but such a pentagon structure is not stable at high temperatures over 1200°C.⁴⁹ Therefore, by comparing the B 1s and N 1s spectra in detail, this peak could be assigned to nitrogen bound with the partially oxidized boron (e.g., BNO moiety).

When the doping temperature is increased to 1500°C (Fig. 2 (b)), a large downshift in the position of the C=C derived peak in B-G15 and NB-G15 can be explained by the increased number of substitutional boron atoms in graphenes.^{41, 42} The intensified peak at 188.0 eV in the B 1s spectra of B-G15 and NB-G15 provides direct evidence for the presence of boron atoms in the form of BC_3 . However, the lack of a shift in the position of the C=C derived peak in N-G15 is due to the substantial removal of quaternary nitrogen from graphene (see the lowered peak intensity in the N 1s spectrum of N-G15), which is consistent with our previous work on the thermal decomposition of nitrogen atoms in carbon nanotubes.⁴⁰ A strong BN-derived peak in the N 1s spectrum of NB-G15 indicates that the BNO moiety in NB-G12 was converted into BN bonding in NB-G15.

Based on detailed XPS studies, a rough schematic doping process (Fig. 3) is proposed for B-, N- and BN- co-doped graphene materials. From the XPS studies, we concluded that a substantial amount of N and BN or BNO moieties were generated in N doped and NB doped graphenes, respectively. In

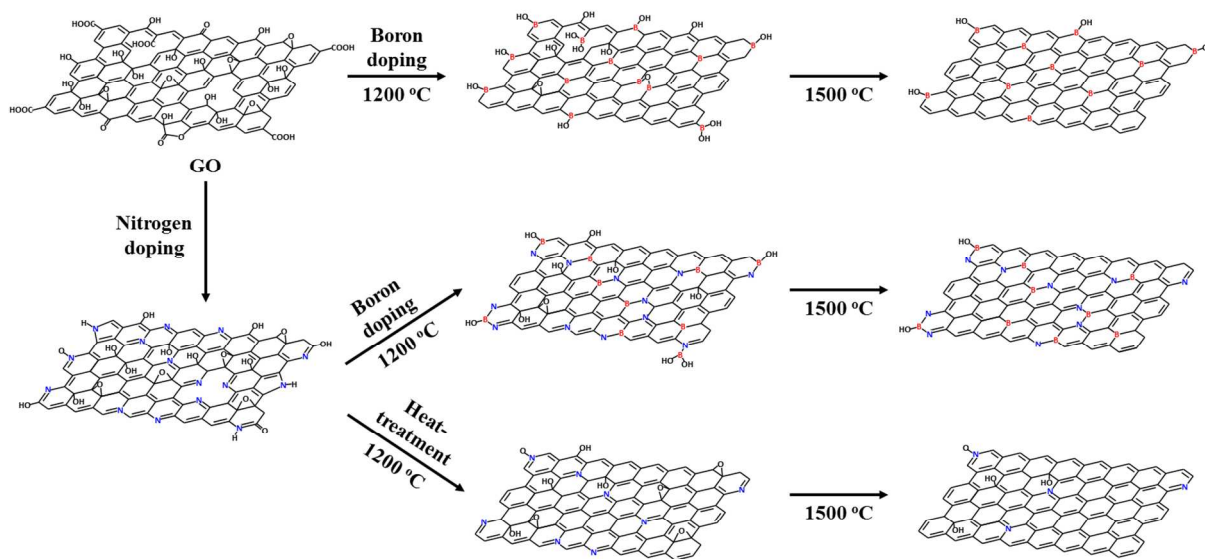


Fig. 3 Schematic illustration of doping behaviours during nitrogen plasma treatment and high temperature thermal diffusion of boron

the case of B- and NB-doped graphenes, a large number of boron atoms are present in the form of B-O bonds. It is reported that the boron atoms in carbon lattices show both a catalytic effect and an inhibition effect on carbon oxidation, because of the redistribution of π electrons and a reduction in the electron density of the active carbon atom, respectively.^{50, 51} Therefore, the introduced boron atoms reduce the electron density of active carbon atoms and prevent the chemisorption of an oxygen atom to a carbon atom, thus resulting in the formation of a B-O bond. Moreover, since carbon atoms at edge-sites possess a higher chemical activity, a large number of the boron atoms in the form of a B-O bond must be located at the edges. We believe that the NB co-doping process changes the configuration of boron or nitrogen from BCO to BN and BNO. In addition, the NB co-doping process is expected to stabilize nitrogen atoms as BN or BNO moieties during high temperature heat treatment. A substantial decrease in the amount of BNO moieties with the increase in temperature up to 1500°C can be explained by the thermal evolution of oxygen-related functional groups as well as by the structural loop formation at edges.

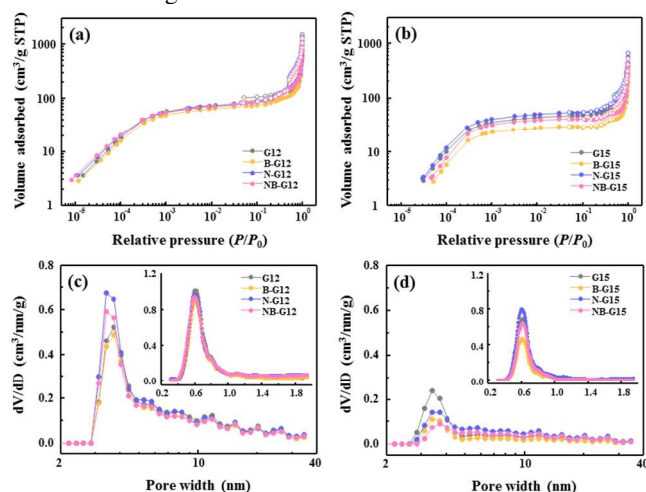


Fig. 4 Nitrogen isotherms of undoped and doped graphenes prepared at 1200°C (a) and 1500°C (b), respectively. Mesopore size distribution evaluated by the QSDFT method using the slit-type pore model is shown in (c) and (d), for samples prepared at 1200°C (c) and 1500°C (d), respectively. The insets in (c) and (d) show the micropore size distribution evaluated by the Horvath-Kawazoe method.

The specific surface area and pore structure of doped and undoped carbons are important factors for understanding their electrochemical performance. Thus the nitrogen isotherm was measured to analyse the pore structure of graphenes (Fig. 4 (a) and (b)). All isotherms of graphenes that were prepared at 1200°C show two distinctive changes; the abrupt rise at low pressure corresponds to the adsorption at micropores (below 2 nm) and a hysteresis at relatively high pressure indicates the existence of mesopores (2 to 50 nm). These micropores could arise from the interlayer spacing between stacked graphenes, whereas mesopores originate from voids among aggregated graphenes. From the nitrogen absorption data of all graphene samples, we calculated the specific surface areas using the Brunauer-Emmett-Teller (BET) method (Table 1) and the pore size distributions using a quenched solid density function theory (QSDFT) method assuming a slit pore model (Fig. 4(c) and 4(d))⁵² and Horvath-Kawazoe (HK) method (micropore, inset of Fig. 4(c) and 4(d)).⁵³ The absence of a difference in S_{BET} and pore structure among the graphene materials that were prepared at 1200°C indicates the absence of a temperature-

dependent morphological effect on the ion adsorption/desorption dynamics. Thus, the changes in electrochemical behaviour for graphene samples that were prepared at 1200°C can be understood only by the effect of heteroatom decorated edges.

Generally, graphenes at 1500°C (Fig. 4 (b)) show relatively low S_{BET} compared with that of graphenes at 1200°C, possibly due to the loop formation at the edges. The S_{BET} in descending order is N-G15 > G15 > B-G15 and NB-G15. A large decrease in S_{BET} of B-G15 and NB-G15 can be explained by the catalytic effect of heteroatoms on graphitization during heat-treatment. Boron atoms can easily diffuse into the graphene lattice and many of the boron atoms were formed to be trapped at the active edge-sites.⁵⁴ With increasing temperature, oxygen atoms were removed from B-O bonding, and then the entrapped boron atoms with a high diffusion rate could promote graphitization, thereby resulting in loop formation at the edges (see Fig. 1 (f-h)). In contrast to boron atoms, quaternary nitrogen atoms (which are stable up to 1500°C) are likely to disturb the graphitization process,⁵⁵ resulting in a high value of S_{BET} . For graphenes that were prepared at 1500°C, the pore structures (i.e., S_{BET} and pore size) are thus strongly dependent on the type of dopants.

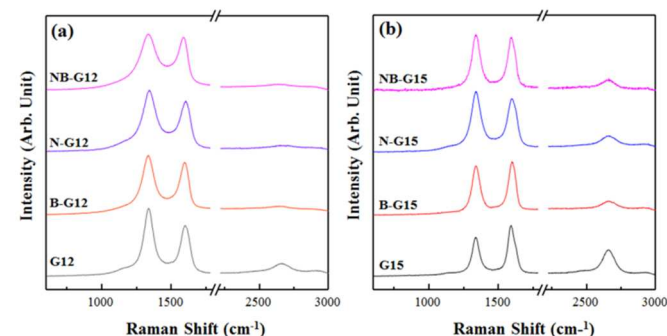


Fig. 5 Raman spectra of undoped and doped graphenes that are prepared at 1200°C (a) and 1500°C (b). Note that the excitation laser wavenumber is 632.8 nm.

It is well known that the edges show a relatively higher interfacial capacitance (F/m^2) than the basal-plane due to their relatively high density of states (DOS).¹⁹⁻²³ Therefore, measurements were made of the ratio of the edge/basal-plane behaviours in undoped and doped graphenes with the help of Raman spectroscopy (Fig. 5). There is a relatively sharp, strong G-band (E_{2g2} graphite mode) around 1585 cm^{-1} and a broad D-band (defect-induced mode) at 1350 cm^{-1} . Thus, the R value ($I_{\text{D}}/I_{\text{G}}$, the integrated intensity of the G-band divided by the integrated intensity of the D-band) indicates the ratio of edge/basal plane to some degree.⁵⁶ All graphene samples treated at 1200°C show an intense D-band, indicating the presence of large amount of defects, such as bonding with heteroatoms, vacancies, and lattice distortions. In order to observe the effect of doping, we summarized the R value and the full width at half maximum (FWHM) intensity of the D-band (Table S1). For graphenes prepared at 1200°C, the doped graphenes exhibit lower R values and higher FWHM than for the undoped graphene. Since the position and shape of the D-band depend on the type of defects, it is expected that heteroatom doping increases the diversity of defect types, therefore broadening the peak.⁵⁷ For graphenes prepared at 1500°C, the B- and NB-doped graphenes have lower R value than the G15 sample. However, G-N15 shows the largest R value. Such changes in the R value and FWHM strongly

support the promotion (boron) or obstruction (nitrogen) effect during the graphitization process caused by heteroatom doping. From Raman studies, it is observed that the active edges in graphenes prepared at 1200°C are decorated by heteroatoms without any change in morphology, whereas the edges in graphenes at 1500°C are energetically stabilized through the formation of loops from the catalytic graphitization effect of boron atoms.

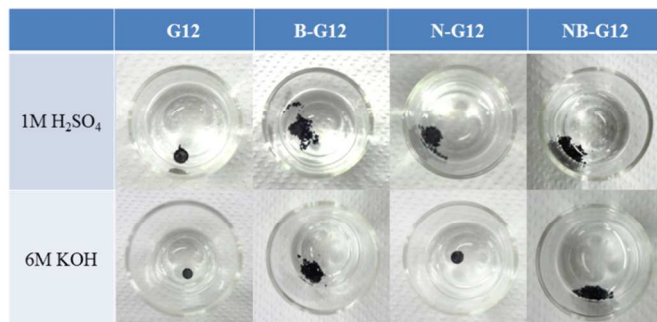


Fig.6 A simple wettability test of undoped and doped graphenes. Graphene sample (1 mg) was shaped into a 4 mm diameter pellet, by applying 3 kN of pressure. Then photos were taken after the pellets were immersed in the electrolyte for 5 seconds.

Since the charge/discharge occurs at the interface between the electrode and the electrolyte, the wettability of the electrode is another important factor affecting the electrochemical performance of active materials. However, there is difficulty in measuring the contact angle of graphenes which are in a powdery form. Therefore, a simple wettability test was carried out for graphene samples that were prepared at 1200°C (Fig. 6). The easily broken and dispersed boron doped graphenes (e.g., B-G12 and NB-G12) in both electrolyte solutions indicates a high affinity with both acidic and alkaline media. On the other hand, undoped graphene (G12) floats as a pellet in solution, suggesting a low affinity with both electrolytes. However, a high affinity with acidic medium was observed for N-G12. The different affinities with the acidic and alkaline media for the doped and undoped graphenes could be explained by the introduction of polar sites by oxygen, nitrogen and boron atoms.^{25, 27}

To understand the effect of heteroatoms on electrochemical behaviour, the cyclic voltammograms (CVs) of undoped and doped graphenes using a three electrode system were measured with a 50 mV/s scan rate (Fig. 7). Here we observed a large dependence of the CVs on the type of electrolytes. For graphene samples that were prepared at 1200°C (Fig. 7 (a)), a large increase in current density and a broad reversible peak are clearly observed in 1 M H₂SO₄ for doped graphene samples, whereas the CV for undoped graphene (G12) shows a rectangular shape. The peaks in B-G12 and NB-G12 are relatively larger than that of N-G12. With increasing temperature up to 1500°C (Fig. 7 (c)), the CV peaks disappear. In 6 M KOH, the oxidation peaks were not observed for G12, B-G12 and NB-G12, whereas small peaks were observed for N-G12 (Fig. 7 (d)). Interestingly, B-G12 and NB-G12 show a large increase of the current density in both acidic and alkaline electrolytes.

In 1M H₂SO₄, the reversible broad peaks can be explained by Faradaic reactions. Thus the increased current density comes from the pseudo-capacitance of the heteroatom functionalities or oxygen functionalities (C-O functionalities). In a protonic electrolyte, a proton exchange reaction such as for quinone/hydroquinone functionalities gives rise to large

pseudo-capacitive behavior.^{37, 58} However, there is no clear difference in the quinone group (287.4 eV) from the C1s spectra (Fig. 2). In addition, the oxygen (O 1s)/carbon (C 1s) ratio for doped graphenes are also similar to that of undoped graphene (0.015, 0.039, 0.018 and 0.030 for G12, B-G12, N-G12 and NB-G12, respectively). The higher value of the (O 1s)/(C 1s) ratio for B-G12 and NB-G12 is due to the fact that many of oxygen atoms are bonded to a boron atom, and thus the amount of oxygen atoms is increased. According to the above result, the effect of oxygen functionalities (C-O) on the pseudo-capacitance cannot explain the observed increase of the current density. Then, this effect could be explained by the evolution of a pseudo-capacitance caused by the chemically introduced heteroatoms. Previous studies on the pseudo-capacitive behaviour of B/N/C carbon revealed that these pseudo-capacitance contributions correspond to the C-B-O or >B-N< moieties.^{29, 59, 60} Even though B-G15 has a large amount of BN moieties, the pseudo-capacitive behaviour is not obvious. Thus, it is noteworthy that heteroatom-related functionalities at edges of graphenes prepared at 1200°C provide a significant contribution to the pseudo-capacitance. Based on our XPS analysis of B-G12 and NB-G12, the pseudo-capacitance from BCO and BNO moieties that are located at edges could be the main reason for the increase of the current density.

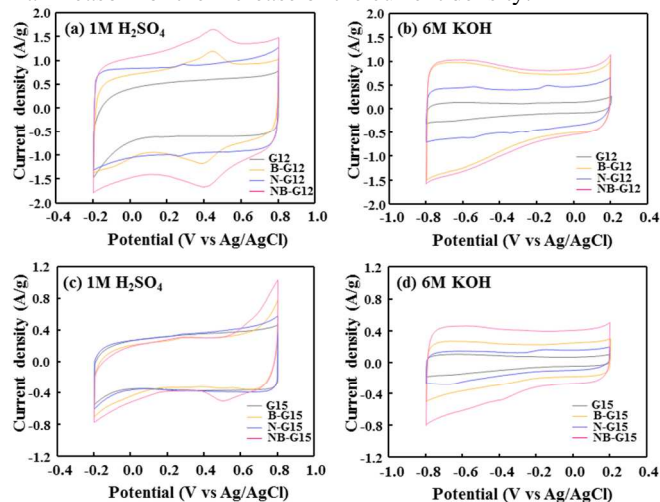


Fig.7 Three-electrode cyclic voltammograms of undoped and doped graphenes prepared at 1200°C (a, b) and 1500°C (c, d). Cyclic voltammograms were obtained using two different electrolytes, 1M H₂SO₄ (acidic, (a), (c)) and 6M KOH (alkaline, (b), (d)). The electrode mass was ca. 10 μg and the scan rate was 50 mV/s.

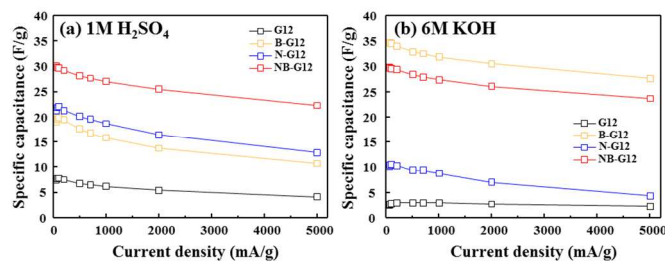


Fig.8 Variation of the specific gravimetric capacitance as a function of current density. (a) and (b) show the specific capacitance in an acidic and an alkaline medium, 1 M H₂SO₄ and 6 M KOH, respectively. Each galvanostatic charge/discharge test was carried out with a voltage limit of 1.0 V and the specific capacitance was calculated from the discharge slope.

In 6 M KOH, the tendency of the capacitance can be partially explained by the wettability of the samples. Therefore, a large increase in the current density for B-G12 and NB-G12 is

likely caused by the increased wettability and pseudo-capacitance. The incorporated boron and oxygen atoms improve the affinity of graphenes with regard to an alkaline medium, resulting in the increase in the magnitude of the accessible surface area.²⁵ In an alkaline medium, the Faradaic reaction involving the quinone/hydroquinone group is not active,⁵⁸ but the reduction of the phenol group and the deprotonation of the carboxyl group showed a quasi-reversible pseudo-capacitance.^{61, 62} Based on XPS analysis there is no large difference in the number of oxygen functionalities (C-O functionalities) for doped graphenes. In addition, NB-G15 shows a large increase in the current density even though the oxygen content is low. From these results, it is clear that the contribution of oxygen functionalities (C-O functionalities) such as that coming from phenol and carboxyl groups is not significant. The large increase in the current density is observed only for B-doped or NB-doped graphenes. Thus, such an increase can be explained by the pseudo-capacitance originated from the BCO and BNO moieties, which are located at the edges of graphenes, without showing any significant pseudo-peak. These results support the fact that doped graphenes have a complex local structure due to boron, nitrogen and oxygen atoms that causes a broadened pseudo-peak over the CV curve.

Table 2 Gravimetric capacitance (C_g), interfacial capacitance (C_s) and capacitance retention and electrical conductivity of undoped and doped graphenes that are prepared at 1200°C.

Sample I.D.	S_{BET} (m ² /g)	1M H ₂ SO ₄			6M KOH			Resistivity (Ω-cm) ^d
		C_g (F/g) ^a	C_s (F/cm ²) ^b	$C_{\text{B5A}}/C_{\text{B0.1A}}$ (%) ^c	C_g (F/g) ^a	C_s (F/cm ²) ^b	$C_{\text{B5A}}/C_{\text{B0.1A}}$ (%) ^c	
G12	343	7.86	2.29	53.3	2.59	0.84	79.9	1.49×10^{-1}
B-G12	301	19.9	6.61	58.3	34.6	11.5	80.1	2.04×10^{-1}
N-G12	342	22.2	6.49	54.0	10.6	3.10	41.5	1.12×10^{-1}
NB-G12	341	29.7	8.71	75.2	29.6	8.68	80.2	6.07×10^{-2}

^a C_g indicates specific gravimetric capacitance at 100 mA/g, ^b C_s is calculated by dividing the specific gravimetric capacitance (C_g) by the specific surface area (S_{BET}), ^c Capacitance retention ($C_{\text{B5A}}/C_{\text{B0.1A}}$ (%)) is calculated by dividing C_g at the current density of 5 A/g by C_g at the current density of 0.1 A/g, ^d Resistivity of the electrode is measured using a four probe method.

Finally, in order to examine the rate performance of doped and undoped graphenes, 2-electrodes galvanostatic charge/discharge measurements were carried out with a voltage limit of 0 - 1.0 V (Figure S4). The specific gravimetric capacitance C_g was calculated from discharge slope using the equation ($C_g = 2 \times I \times \Delta t / (\Delta V \times m)$, m : mass of electrode). Figure 8 shows the current density dependence of the specific gravimetric capacitance in 1 M H₂SO₄ (Fig. 8 (a)) and 6 M KOH (Fig. 8 (b)). In both systems, heteroatom-doped graphenes show higher capacitance than the undoped materials. The enhancement in the capacitance also strongly depends on the type of electrolytes; NB-G12 shows the highest capacity in an acidic medium, whereas B-G12 shows the highest capacitance in an alkaline medium. In order to analyse the electrochemical performance, specific gravimetric capacitance (C_g), interfacial capacitance ($C_s = C_g / S_{\text{BET}}$),²⁷⁻²⁹ capacitance retention (= C_g (5 A/g) / C_g (0.1 A/g)), and electric resistivity of the electrode were tabulated (Table 2). Doped graphenes show 4–10 times higher C_g and C_s than the corresponding undoped materials, because of the evolution of pseudo-capacitance and the improved wettability caused by heteroatom doping. NB-G12 and B-G12 show excellent capacitance retention ability in an alkaline medium. In the high current density region, it is known that the diffusion of electrolyte ions, the transport of electrons and the charge transfer dynamics of the Faradaic reaction of pseudo-capacitance all limit the capacitance.^{24, 28} For NB-G12, the boron and oxygen atom-related moieties improve the affinity of the sample with the electrolyte, and the boron and nitrogen atoms at the trigonal sites improve the

electrical conductivity, thereby resulting in a high capacitance retention in both acidic and alkaline media. Such kind of explanation is well consistent with the data obtained from electrochemical impedance spectroscopy (Fig. S5). In contrast to NB-G12, N-G12 shows low capacitance retention ability in alkaline media. Even though incorporated nitrogen atoms enhance the electrical conductivity of graphene, such a low rate capability can be explained by two factors: a low affinity of these materials with an alkaline medium and a slow Faradaic reaction. However, G12 shows a high rate capability, even though it has a low affinity with alkaline medium. Thus it is concluded that the low rate capability in N-doped graphene is due to a slow charge transfer during the Faradaic reaction.

Conclusions

Heteroatom-doped graphene samples were prepared by thermally treating GO in boron rich environment at 1200 and 1500°C and by subjecting GO to nitrogen plasma. The electrochemical characterization of these materials was also carried out. Based on detailed high-resolution TEM observations, doped graphenes that were prepared at 1200°C kept open heteroatom-functionalized edges, whereas doped graphenes that were prepared at 1500°C showed loop formation at their edges. From XPS analysis, we found that boron atoms that are predominately located at the edge-sites were oxidized and formed a BCO moiety, while nitrogen atoms were incorporated into the graphene lattice (quaternary nitrogen). For NB co-doping, nitrogen atoms were present as the BNO moiety at the edges and as a BN moiety in the basal-plane. We observed a large increase in the specific capacitance for B-G12 and N-G12 samples. N functionalities and the BCO moiety in doped graphene improved the wettability and contributed to the pseudo-capacitance. The best capacitive performance in both acidic and alkaline media for NB-G12 could be explained by the BNO moieties likely to be at the edges. We therefore believe that edge-functionalization and NB co-doping provides a powerful tool for achieving both high capacitance and rate capability, and the approach we developed is easily applicable to other types of carbon materials.

Experimental

Preparation of Graphene Oxide

Highly crystalline Madagascar graphite was chosen to synthesize GO. The GO was prepared using a modified Hummers method.³⁸ First, Madagascar graphite (ca. 10g) was mixed with 98% sulphuric acid (60 ml). The suspension was heated up to 80-90°C under stirring, and then phosphorous pentoxide (10g) was added slowly. Next potassium persulfate were added. The slurry was stirred for 4.5 h and followed by slow addition of distilled water. The mixture was cooled, decanted, washed, filtered, and then dried overnight. The intercalated graphite (6g) was added to H₂SO₄ (230 ml) and the mixture was cooled. When potassium permanganate (30g) was added slowly under stirring, a green permanganic acid solution was observed. (Caution, permanganic acid solutions react violently with organic solvents and should not be heated above 55°C). The mixture was heated slowly to 40°C for 2 h. Finally, water was added slowly up to 1L and hydrogen peroxide (25 mL) was added drop by drop until the colour turned from brown to yellow. The mixture was stirred for 2 h and left overnight and decanted. The solution was washed with

hydrochloric acid (10%), centrifuged and dispersed in distilled water (1L). The dispersion-centrifugation step was repeated three times. Finally, we obtained a sponge-like sample through a freeze drying of the GO slurry.

Structural Characterization

The structures of thermally reduced and heteroatom-doped graphenes were characterized by using a field emission-scanning electron microscope (FE-SEM, JEM-6335F, JEOL, acceleration voltage: 10kV), and a double Cs-corrector equipped high resolution transmission electron microscope (Cs-HR-TEM, JEM2100F, JEOL, acceleration voltage: 80kV). Surface elemental analysis was carried out by X-ray photoelectron spectroscopy (XPS, Axis-Ultra, Shimadzu-Kratos), using a monochromatic X-ray source coming from an Al target (15 kV, 15 mA). The pore structure was analyzed by nitrogen adsorption. Nitrogen adsorption isotherms were collected by ASAP 2020 (Shimadzu Micrometrics) at liquid nitrogen temperature (77K). The crystallinity was evaluated by Raman spectroscopy using a He-Ne laser (λ : 632.8 nm) under a microscope (HORIBA Jobin-Yvon: T64000). The nitrogen plasma treatment was carried out using radio-frequency etching system (Samco, FA-1).

Electrochemical Analysis

The graphene sample was dispersed in isopropyl alcohol under sonication and then a certain amount of the resulting suspension was dropped onto the glassy carbon electrode (diameter = 3 mm). The electrochemical properties were determined with a multi-channel potentiostat/galvanostat (VSP, Biologic). For the 3-electrode cell experiments, an Ag/AgCl reference electrode and a Pt counter electrode were used. The electrochemical test was carried out in a 1 M H₂SO₄ or in a 6 M KOH solution with a scanning rate of 50 mV/s. In the case of a 2-electrode system, the two electrodes were prepared by mixing 75% of graphene and 25% of polytetrafluoroethylene. The cell was charged up to 1.0 V and the specific discharge capacitance was measured using a wide range of current densities from 20 to 5000 mA/g.

Acknowledgements

KF acknowledges the support through a Grant-in-Aid for Japan Society for the Promotion of Science (JSPS) fellows (No. 24-10710). R.C.S and M.T. acknowledge the support of the JST. Y.A.K and K.S.Y acknowledge the support from Global Research Laboratory (K2090300202412E010004010) through the National Research Foundation of Korea (NRF) funded by the Ministry of Science, ICT (Information and Communication Technologies) and Future Planning. M.S.D acknowledges support from US NSF DMR 10-04147.

Notes and references

^aFaculty of Engineering, Shinshu University, 4-17-1 Wakasato, Nagano 380-8553, Japan

^bResearch Center for Exotic Nanocarbons (JST), Shinshu University, Wakasato 4-17-1, Nagano 380-8553, Japan.

^cSchool of Polymer Science and Engineering & Alan G. MacDiarmid Energy Research Institute, Chonnam National University, 77 Yongbong-ro, Buk-gu, Gwangju 500-757, Korea. Fax: +82-62-530-1779; Tel: +82-62-530-1871; E-mail: yak@jnu.ac.kr

^dDepartment of Physics, Department of Materials Science and Engineering & Materials Research Institute, The Pennsylvania State University, 104 Davey Lab., University Park, PA 16802-6300, USA

^eDepartment of Electrical Engineering and Computer Science and Department of Physics, Massachusetts Institute of Technology, Cambridge, Massachusetts 02139-4307, USA

† Electronic Supplementary Information (ESI) available: [SEM image, Low magnification TEM image and detailed of Raman analysis result]. See DOI: 10.1039/b000000x/

- Citations here in the format A. Name, B. Name and C. Name, *Journal Title*, 2000, **35**, 3523; A. Name, B. Name and C. Name, *Journal Title*, 2000, **35**, 3523.
- K. S. Novoselov, A. K. Geim, S. V. Morozov, D. Jiang, Y. Zhang, S. V. Dubonos, I. V. Grigorieva, A. A. Firsov, *Science*, 2004, **306**, 666-669.
- A. K. Geim, K. S. Novoselov, *Nature Mater.*, 2007, **6**, 186-191.
- J. Hou, Y. Shao, M. W. Ellis, R. B. Moore, B. Yi, *Phys. Chem. Chem. Phys.*, 2011, **13**, 15384-25402.
- Y. Huang, J. Liang, Y. Chen, *Small*, 2012, **8**, 1805-1834.
- H.-J. Choi, S.-M. Jung, J.-M. Seo, D.-W. Chang, L. Dai, J.-B. Baek, *Nano Energy*, 2012, **1**, 534-551.
- C. Xu, B. Xu, Y. Gu, Z. Xiong, J. Sun, X. S. Zhao, *Energ. Environ. Science*, 2013, **6**, 1388-1414.
- E. Frackowiak, *Phys. Chem. Chem. Phys.*, 2007, **9**, 1774-1785.
- B. E. Conway, Kluwer Academic/Plenum, New York, 1999.
- C. Liu, H. M. Cheng, *J. Phys. D: Appl. Phys.*, 2005, **38**, R231-R252.
- C. G. Liu, Z. N. Yu, D. Neff, A. Zhamu, B. Z. Jang, *Nano Lett.*, 2010, **10**, 4863-4868.
- J. R. Miller, R. A. Outlaw, B. C. Holloway, *Science*, 2010, **329**, 1637-1639.
- J. J. Yoo, K. Balakrishnan, J. Huang, V. Meunier, B. G. Sumpter, A. Srivastava, M. Conway, A. L. Reddy, J. Yu, R. Vajtai, P. M. Ajayan, *Nano Lett.* 2011, **11**, 1423-1427.
- Y. Zhu, S. Murali, M. D. Stoller, K. J. Ganesh, W. Cai, P. J. Ferreira, A. Pirkle, R. M. Wallace, K. A. Cychoz, M. Thommes, D. Su, E. A. Stach, R. S. Ruoff, *Science*, 2011, **332**, 1537-1541.
- M. F. El-Kady, V. Strong, S. Dubin, R. B. Kaner, *Science*, 2012, **335**, 1326-1330.
- Z. Niu, L. Zhang, B. Zhu, H. Dong, X. Chen, *Adv. Mater.*, 2013, **25**, 4035-4042.
- K. Nakada, M. Fujita, G. Dresselhaus, M. S. Dresselhaus, *Phys. Rev. B* 1996, **54**, 17954-17961
- K. Suenaga, M. Koshino, *Nature*, 2010, **468**, 1088-1090.
- C. Tao, L. Jiao, O. V. Yazyev, Y.-C. Chen, J. Feng, X. Zhang, R. B. Capaz, J. M. Tour, A. Zettl, S. G. Louie, H. Dai, M. F. Crommie, *Nat. Phys.*, 2011, **7**, 616-620.
- J. P. Randin, E. Yeager, *J. Electrochem. Soc.*, 1971, **118**, 711-714.
- K. Kinoshita, Carbon, Electrochemical and Physicochemical Properties. Wiley Interscience, New York, 1987.
- I. Y. Jang, H. Ogata, K. C. Park, S. H. Lee, J. S. Park, Y. C. Jung, Y. J. Kim, Y. A. Kim, M. Endo, *J. Phys. Chem. Lett.*, 2010, **1**, 2099-2103.
- Y. J. Kim, C. M. Yang, K. C. Park, K. Kaneko, Y. A. Kim, M. Noguchi, T. Fujino, S. Oyama, M. Endo, *ChemSusChem*, 2012, **5**, 535-541.
- W. Yuan, Y. Zhou, Y. Li, C. Li, H. Peng, J. Zhang, Z. Liu, L. Dia, G. Shi, *Sci. Rep.*, 2013, **3**, 2248.
- K. Jurewicz, K. Babel, A. Źiółkowski, H. Wachowska, *Electrochimica Acta*, 2003, **48**, 1491-1498.
- G. Lota, B. Grzyb, H. Machnikowska, J. Machnikowski, E. Frackowiak,

- Chem. Phys. Lett.*, 2005, **404**, 53-58.
- 26 S. Sepehri, B. B. Garcia, Q. Zhang, G. Cao, *Carbon*, 2009, **47**, 1436-1443.
- 27 H. Guo, Q. Gao, *J. Power Sources*, 2009, **186**, 551-556.
- 28 T. Kwon, H. Nishihara, H. Itoi, Q. H. Yang, T. Kyotani, *Langmuir*, 2009, **25**, 11961-11968.
- 29 H. Konno, T. Ito, M. Ushiro, K. Fushimi, K. Azumi, *J. Power Sources*, 2010, **195**, 1739-1746.
- 30 T. Tomko, R. Rajagopalan, P. Aksoy, H. C. Foley, *Electrochimica Acta*, 2011, **56**, 5369-5375.
- 31 T. Tsubota, K. Takenaka, N. Murakami, T. Ohno, *J. Power Sources*, 2011, **196**, 10455-10460.
- 32 D. Hulicova-Jurcakova, A. M. Puziy, O. I. Poddubnaya, F. Suarez-Garcia, J. M. D. Tascon, G. Q. Lu, *J. Am. Chem. Soc.*, 2009, **131**, 5026-5027.
- 33 S. Shiraiishi, M. Kibe, T. Yokoyama, H. Kurihara, N. Patel, A. Oya, Y. Kaburagi, Y. Hishiyama, *Appl. Phys. A*, 2006, **82**, 585-591.
- 34 D. W. Wang, F. Li, Z. G. Chen, G. Q. Lu, H. M. Cheng, *Chem. Mater.*, 2008, **20**, 7195-7200.
- 35 J. Han, L. L. Zhang, S. Lee, J. Oh, K.-S. Lee, J. R. Potts, J. Ji, X. Zhao, R. S. Ruoff, S. Park, *ACS Nano*, 2013, **7**, 19-26.
- 36 C.-T. Hsieh, H. Teng, *Carbon*, 2002, **40**, 667-674.
- 37 K. Okajima, K. Ohta, M. Sudoh, *Electrochimica Acta*, 2005, **50**, 2227-2231.
- 38 N. I. Kovtyukhova, P. J. Ollivier, B. R. Martin, T. E. Mallouk, S. A. Chizhik, E. V. Buzaneva, A. D. Gorchinskiy, *Chem. Mater.* 1999, **11**, 771-778.
- 39 D. Long, W. Li, W. Qiao, J. Miyawaki, S.-H. Yoon, I. Mochida, L. Ling, *Nanoscale*, 2011, **3**, 3652-3656.
- 40 K. Fujisawa, T. Tojo, H. Muramatsu, A. L. Elias, S. M. Vega-Diaz, F. Tristan-Lopez, J. H. Kim, T. Hayashi, Y. A. Kim, M. Endo, M. Terrones, *Nanoscale*, 2011, **3**, 4359-4364.
- 41 J. Tarabek, L. Kavan, L. Dunsch, M. Kalbac, *J. Phys. Chem. C*, 2008, **112**, 13856-13861.
- 42 Y. A. Kim, K. Fujisawa, H. Muramatsu, T. Hayashi, M. Endo, T. Fujimori, K. Kaneko, M. Terrones, J. Behrends, A. Eckmann, C. Casiraghi, K. S. Novoselov, R. Saito, M. S. Dresselhaus, *ACS Nano*, 2012, **6**, 6293-6300.
- 43 T. Shirasaki, A. Derre, M. Menetrier, A. Tressaud, S. Flandrois, *Carbon*, 2000, **38**, 1461-1467.
- 44 S. Jacques, A. Guette, X. Bourrat, F. Langlais, C. Guimon, C. Labrugere, *Carbon*, 1996, **34**, 1135-1143.
- 45 X. Gouin, P. Grange, L. Bois, P. L'Haridon, Y. Laurent, *J. Alloys Compd.*, 1995, **224**, 22-28.
- 46 K. A. Simonov, N. A. Vinogradov, M. L. Ng, A. S. Vinogradov, N. Martensson, A. B. Preobrajenski, *Surface Science*, 2012, **606**, 564-570.
- 47 J. R. Pels, F. Kapteijn, J. A. Moulijn, Q. Zhu, K. M. Thomas, *Carbon*, 1995, **33**, 1641-1653.
- 48 E. Raymundo-Pinero, D. Cazorla-Amoros, A. Linares-Solano, J. Find, U. Wild, R. Schlogl, *Carbon*, 2002, **40**, 597-608.
- 49 Y. Ma, S. Jiang, G. Jian, H. Tao, L. Yu, X. Wang, X. Wang, J. Zhu, Z. Hu, Y. Chen, *Energy Environ. Sci.*, 2009, **2**, 224-229.
- 50 X. Ma, Q. Wang, L. Q. Chen, W. Cermignani, H. H. Schobert, C. G. Pantano, *Carbon*, 1997, **35**, 1517-1525.
- 51 L. R. Radovic, M. Karra, K. Skokova, P. A. Thrower, *Carbon*, 1998, **36**, 1841-1854.
- 52 P. I. Ravikovitch, A. V. Neimark, *Langmuir*, 2006, **22**, 11171-11179.
- 53 G. Horvath, K. Kawazoe, *J. Chem. Eng. Jpn.*, 1983, **16**, 470-475.
- 54 A. Oya, R. Yamashita, S. Otani, *Fuel*, 1979, **58**, 495-500.
- 55 M. Inagaki, H. Tachikawa, T. Nakahashi, H. Konno, Y. Hishiyama, *Carbon*, 1998, **36**, 1021-1025.
- 56 L. G. Cancado, K. Takai, T. Enoki, M. Endo, Y. A. Kim, H. Mizusaki, L. N. Coelho, R. Magalhães-Paniago, A. Jorio, M. A. Pimenta, *Appl. Phys. Lett.*, 2006, **88**, 163106.
- 57 Q. H. Yang, P. X. Hou, M. Unno, S. Yamauchi, R. Saito, T. Kyotani, *Nano Lett.*, 2005, **5**, 2465-2469.
- 58 H. A. Andreas, B. E. Conway, *Electrochimica Acta*, 2006, **51**, 6510-6520.
- 59 T. Ito, M. Ushiro, K. Fushimi, K. Azumi, H. Konno, *TANSO*, 2009, **239**, 156-161.
- 60 M. Inagaki, H. Konno, O. Tanaike, *J. Power Sources*, 2010, **195**, 7880-7903.
- 61 E. Frackowiak, F. Beguin, *Carbon*, 2001, **39**, 937-950.
- 62 D. W. Wang, F. Li, M. Liu, H. M. Cheng, *New Carbon Mater.*, 2007, **22**, 307-314.

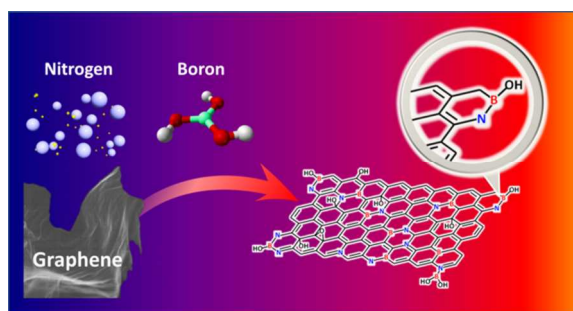
ARTICLE

The table of contents entry

Keywords (Graphene, Doping, Open Edge, Supercapacitor)

Kazunori Fujisawa, Rodolfo Cruz-Silva, Kap-Seung Yang, Yoong Ahm Kim,* Takuya Hayashi, Morinobu Endo, Mauricio Terrones, Mildred S. Dresselhaus

Title: Importance of Heteroatom-Decorated Edges in Chemically-Doped-Graphene for Supercapacitor Applications



We demonstrated the importance of open, heteroatom-decorated open edges in graphene-based supercapacitor applications.